Supporting Information

Buller et al. 10.1073/pnas.1516401112

SI Materials and Methods

Cloning, Expression, and Purification of *Pf*TrpA and *Pf*TrpB. The gene encoding *Pf*TrpB (UNIPROT ID Q8U093) was obtained as a single gBlock, codon-optimized for *E. coli*, and cloned using Gibson Assembly (40) into pET22(b)+ between restriction sites *Nde*I and *Xho*I in frame with the C-terminal his6-tag for expression in *E. coli* BL21 *E. cloni* EXPRESS cells (Lucigen). The gene coding for *Pf*TrpA (UNIPROT ID Q8U094) was treated in the same manner as described above, but the his6-tag was omitted. For heterologous protein expression of *Pf*TrpA and *Pf*TrpB, 5 mL TB_{amp} was inoculated with single BL21 *E. cloni* colonies and incubated overnight at 37 °C and 250 rpm. The overnight cultures were used to inoculate 500-mL TB_{amp} expression cultures to an initial OD_{600} of 0.1. After shaking at 250 rpm and 37 °C for ∼3 h or until an OD_{600} of 0.8 was reached, the cultures were chilled on ice for 20 min. The expression was induced by the addition of 500 mM IPTG to a final concentration of 1 mM in the chilled cultures that then continued to grow at 250 rpm and 20 °C for another 20 h. Cells were harvested at 4 °C and 5,000 × *g* for 10 min; the pellets were frozen at –20 °C until further use. For purification, frozen cell pellets of *Pf*TrpB were thawed at room temperature and resuspended in 50 mM phosphate buffer, pH 8, with 20 mM imidazole and 100 mM NaCl (buffer A) with 100 μM PLP. After lysis with BugBuster (Novagen) according to the manufacturer's recommendations, the cells were centrifuged at 20,000 × *g* and 4 °C for 10 min. The lysate was then incubated at 75 °C for 10 min, centrifuged again as described above, and applied to a 1-mL HisTrap HP column. The purification was performed with an AKTA purifier FPLC system (GE Healthcare). *Pf*TrpB eluted during a linear gradient from buffer A to buffer B (50 mM phosphate buffer with 500 mM imidazole and 100 mM NaCl, pH 8) at 140 mM imidazole. Purified *Pf*TrpB was desalted into 50 mM phosphate buffer, pH 8, frozen in liquid N_2, and stored at –80 °C until further use.

Frozen cell pellets containing heterologously expressed *Pf*TrpA were thawed at room temperature and resuspended in 50 mM Tris (pH 8.0). After lysis with BugBuster, heat treatment, and centrifugation as described for *Pf*TrpB, the cleared lysate was passed manually through a 1-mL Q HP HiTrap column, and the flow-through containing *Pf*TrpA was collected. Solid ammonium sulfate was slowly added to the *Pf*TrpA-containing flow through while stirring on ice. After a final concentration of 35% was reached, the lysate was allowed to stir for another 2 h on ice and was then centrifuged at 20,000 × *g* and 4 °C for 30 min. The cleared ammonium sulfate-treated solution was loaded on a 5-mL pre-equilibrated [buffer B: 35% ammonium sulfate, 50 mM phosphate buffer (pH 8)] phenyl Sepharose HP HiTrap column using an AKTA purifier FPLC. TrpA eluted in a linear gradient with buffer A [50 mM phosphate buffer (pH 8)] at 2.5% ammonium sulfate and was then buffer exchanged into 50 mM phosphate buffer, pH 8, and frozen at –80 °C until further use. To obtain highly pure wild-type complex (TrpA and B), we combined purified TrpB with purified TrpA in a 1:2 ratio, applied this mixture to a 1-mL HisTrap HP column, and purified the formed complex via TrpB's his6-tag (Fig. S6).

Protein concentrations were determined via the Bradford assay (Bio-Rad).

Library Construction. The error-prone PCR library for generation 1 was constructed with 300 μM $MnCl_2$ and had an error rate of 1.7 missense mutations per gene among sequenced hits. Initial error-prone PCR libraries for generation 3 were constructed with the Mutazyme II kit (Stratagene) using 100–300 ng DNA. A larger library using 200 ng DNA was selected based on its retention of function rate: 40% of clones had activity not less than 40% less than wild type. This library had an error rate of 1.8 missense mutations per gene among sequenced hits. DNA shuffling was performed to recombine twelve activating mutations, which were distributed over two gBlocks (block 1: W2R, F35S, M123V, N166D, M233V, and T292S; block 2: E17G, I68V, M144T, L182P, F274S, and T312A). These two gBlocks and the wild-type gBlock served as template for DNA shuffling following a modified protocol of Stemmer (41). The resulting library was cloned into pET22(b)+ between restriction sites *Nde*I and *Xho*I in frame with the C-terminal his-tag for expression in *E. coli* BL21 *E. cloni* EXPRESS cells.

Due to low recombination frequency of the DNA shuffling library, a recombination library of mutations found at residues M123, M144, N166, L182, M233, F274, and T292 (generation 2) was constructed using SOE PCR (42). The mutagenesis primers encoded the desired mutations and also the corresponding wild-type sequences. Because the distances between some of the target sites would have resulted in very short fragments, we built the library in two steps. During the first step, we generated five fragments encompassing residues M123, N166, M233, and T292 using Phusion polymerase according to the manufacturer's recommendations. The fragments were then *Dpn*I-digested, gel-purified, and used as template for the subsequent assembly PCR using the flanking primers only. The assembly PCR product served as template for a second round of PCRs generating the fragments carrying the remaining mutations, followed by the same procedure as described above. The final assembly product was cloned into pET22(b)+ between restriction sites *Nde*I and *Xho*I in frame with the C-terminal his-tag for expression in *E. coli* BL21 *E. cloni* EXPRESS cells.

High-Throughput Screening. For high-throughput expression, BL21 *E. cloni* EXPRESS cells carrying *Pf*TrpB wild-type and variant plasmids were grown in 96-well deep-well plates in 300 μL TB_{amp} at 37 °C and 80% humidity with shaking at 250 rpm overnight. TB_{amp} expression cultures (630 μL) were inoculated with 20 μL of the overnight cultures and continued to grow at 37 °C and 80% humidity with shaking at 250 rpm for 3 h. Expression was induced with the addition of ITPG to a final concentration of 1 mM to cold-shocked (20 min on ice-water bath) cultures. The expression continued for another 20 h at 20 °C with shaking at 250 rpm. Cells were then centrifuged at 4,000 × *g* for 10 min and frozen at –20 °C overnight. For screening, cells were allowed to thaw at room temperature and then lysed in lysis buffer (400 μL per well of 200 mM phosphate buffer, pH 8, with 1 mg/mL lysozyme, 40 μM PLP, and ∼0.05 mg/mL DNase I) for 1 h at 37 °C. After centrifugation at 5,000 × *g* for 20 min, a 160-μL aliquot of the lysate was transferred into PCR plates (USA Scientific), heat-treated for 1 h at 75 °C, and then spun again at 1,000 × *g* and 4 °C for 30 min. After the addition of 160-μL assay buffer (200 mM phosphate buffer, 20 mM indole, 0.75 mM L-serine, pH 8) to 40 μL of cleared, heat-treated lysates in UV-transparent assay plates (Evergreen Scientific), formation of L-tryptophan took place at 75 °C for up to 1 h (generation 1:1 h; generations 2 and 3:6 min). The reactions were then quenched in an ice-water bath, and the amount of L-tryptophan formed was recorded at 290 nm with a plate reader (Tecan Infinite M200).

Kinetics. *Pf*TrpB activity (k_{cat}) was measured by monitoring tryptophan formation in a UV1800 Shimadzu spectrophotometer (Shimadzu) at 75 °C over 1 min at 290 nm using $\Delta\varepsilon_{290} = 1.89\ mM^{-1}{\cdot}cm^{-1}$ (15). The assay buffer contained 200 mM potassium phosphate,

pH 8, and 5 μM PLP. Michaelis–Menten constants (K_M) for indole were determined using a concentration range from 0.4 to 0.015 mM indole with the concentration of L-serine fixed at 25 mM. K_M values for L-serine were measured with a concentration range from 50 to 0.5 mM L-serine with the concentration of indole fixed at 250 μM. Data were fit using an in-house nonlinear least-squares algorithm to the Michaelis–Menten equation implemented in MATLAB.

UV-Vis Spectroscopy. Spectra were collected between 550 and 250 nm on a UV1800 Shimadzu spectrophotometer using 20 μM of enzyme in 200 mM potassium phosphate (pH 8.0) in a quartz cuvette. Samples were incubated at 75 °C for >3 min to ensure a stable temperature was reached. Stage 1 of the reaction was initiated by addition of 20 mM L-serine, and the spectra were measured in <10 s to limit production of pyruvate from deamination of L-serine, which absorbs at 320 nm.

Substrate Selectivity. Purified enzyme was used to measure the relative rate of *Pf*TrpS and *Pf*TrpB^{0B2} NCAA production compared with *Pf*TrpB. The 225-μL reactions were set up in duplicate with 20 mM L-serine and 20 mM indole analog (Fig. 5*A*) in 200 mM potassium phosphate (pH 8.0) with 5% DMSO. Assays were set up in glass HPLC vials (to prevent absorption of indole into the reaction vessel) and incubated at 75 °C for 1 h and quenched with addition of 775 μL 50% acetonitrile. Quenched reactions were transferred to an Eppendorf tube, spun for 10 min at 14,000 × *g* and 4 °C to remove precipitated protein, and the supernatant was transferred to fresh HPLC vials. The concentration of enzyme was adjusted to prevent reactions from running to completion. Relative rates were computed by measuring the ratio of the product peaks measured via UHPLC-MS (Agilent 1290 with 6140 MS detector) at 280 nm and then normalizing for the enzyme concentration.

Thermostability Measurements. To determine the temperature where 50% of enzymes are rendered inactive (T_{50}s), 5 μM of *Pf*TrpB wild type and 1 μM of its variants were incubated at varying temperature ranges (wild type: 80–99 °C; variants 75–95 °C) for 1 h. After quenching on ice, the residual activity was measured as described above.

Crystallography. Freshly purified *Pf*TrpB (described above) was buffer exchanged against 20 mM Hepes (pH 7.85) with 5% glycerol and frozen at −80 °C until further use. Sparse matrix screening was performed using an Art Robbins Gryphon Nano crystallization robot using 0.2 μL of 11 mg/mL *Pf*TrpB with 40 μM PLP and 0.2 μL of well solution. Crystals were found in a solution of 25% PEG3350 and 0.1 M Na Hepes (pH 7.5) after 3 d. Crystals were then routinely grown as sitting drops against a 1-mL reservoir of 15–25% PEG3350 and 0.1 M Na Hepes (pH 7.85) with mother liquor comprised of 1.5 μL of 8.0 mg/mL *Pf*TrpB and 1.5 μL of well solution. Ligand-bound structures were determined by soaking crystals of *Pf*TrpB with 15 mM L-tryptophan or 100 mM L-serine for 2 min. Crystals were cryoprotected through oil immersion in Fomblin Y (Sigma) and flash-frozen in liquid N_2 until diffraction. Diffraction data were collected remotely at the Stanford Synchrotron Radiation Laboratories on beamline 12-2. Crystals routinely diffracted at or below 2.0 Å, and the data were integrated and scaled using XDS (43) and AIMLESS (44). A resolution cutoff of CC1/2 > 0.3 was applied along the strongest axis of diffraction (44, 45). These data contributed to model quality as judged by R_{free} in the final bin <0.4. Structures were solved using molecular replacement with PHASER, as implemented in CCP4 (46, 47). The search model comprised a single monomer of *Pf*TrpB (PDB ID code 1V8Z) (21) subjected to 10 cycles of geometric idealization in Refmac5 and removal of all ligands. Model-building was performed in Coot (48) beginning with data processed at 2.4 Å, followed by subsequent inclusion of increasingly higher-resolution shells of data with relaxed geometric constraints. This procedure was particularly important for the structures of L-tryptophan- and L-serine-bound *Pf*TrpB, which contained a large rigid body motion of the COMM domain. Refinement was performed using REFMAC5 (49). The MolProbity server was used to identify rotamer flips and to identify clashes (50). After the protein, ligand, and solvent atoms were built, TLS operators were added to refinement, which resulted in substantial improvements in R_{free} for the models. Crystallographic and refinement statistics are reported in Table S3.

A similar procedure was used for the crystal structure of *Pf*TrpS, with a protein concentration of 4.0 mg/mL. Sparse matrix screening identified crystals grew in 20% PEG 3350 and 0.2 M Na citrate. Crystals were routinely grown in 24-well format with 16–20% PEG 3350 and 0.15–0.2 M Na citrate. Cryoprotection was achieved by the addition of 25% glycerol and flash-frozen in liquid N_2. Crystals regularly diffracted to ∼3.0 Å, and a single crystal was found that diffracted to 2.76 Å. A molecular replacement search model was made using an αβ-dimer of *Pf*TrpS (PDB ID code 1WDW) (22). Model-building proceeded as described above. Data in the final bin were weak, but contributed to model quality as measured by R_{free} < 0.4 in the final bin. Coordinates are deposited in the Protein Data Bank with ID codes 5E0K (*Pf*TrpS), 5DVZ (*Pf*TrpB), 5DW0 (Ser-bound *Pf*TrpB), and 5DW3 (Trp-bound *Pf*TrpB).

Identification of Nonnatural Amino Acid Products. The identities of the amino acid products were confirmed by ^{1}H NMR and LRMS. Proton NMR spectra were recorded on a Varian 300-MHz or Bruker 400-MHz spectrometer. Proton chemical shifts are reported in parts per million (δ) relative to tetramethylsilane and calibrated using the residual solvent resonance (DMSO, δ 2.50 ppm; CD_3OD, δ 3.31 ppm; D_2O, δ 4.79 ppm). Data are reported as follows: chemical shift (multiplicity [singlet (s), doublet (d), doublet of doublets (dd), doublet of doublets of doublets (ddd), triplet (t), triplet of doublets (td)], coupling constants [Hz], integration). Fluorine NMR spectra were recorded on a 300-MHz (282 MHz) spectrometer without proton decoupling. Fluorine chemical shifts are reported in ppm relative to $FCCl_3$ (δ 0.00 ppm) and were calibrated automatically by the spectrometer using the solvent deuterium lock signal. Low-resolution mass spectra were obtained using an Agilent 1290 UHPLC-LCMS. The optical purity of the products was estimated by derivatization with FDNP-alanamide as described below.

Reaction with heat-treated lysate. All reactions were conducted using *Pf*TrpB^{0B2}, which was prepared by heat treatment as described in *SI Materials and Methods, Cloning, Expression, and Purification of PfTrpA and PfTrpB*. The protein was used as a solution in potassium phosphate buffer (50 mM, pH 8) and was found to have a concentration of 134 μM, as determined by specific activity (Table 1). Serine and PLP were used as aqueous solutions (500 mM and 15 mM, respectively).

A 6-mL crimp vial was charged sequentially with the indole analog (50 μmol), dimethyl sulfoxide (50 μL), serine (100 μL), and PLP (3.3 μL). The resulting suspension was diluted with 772 μL of potassium phosphate buffer (200 mM, pH 8). Finally, the enzyme solution was added, and the vial was sealed and immersed in an oil bath that had been equilibrated to 75 °C. After 12 h, the reaction mixture was allowed to cool to room temperature, and then purified directly on C-18 silica (20 mL column volume) with 0–50% methanol/H_2O.

Determination of optical purity. The amino acids were used as 0.2-M solutions in 1 N aqueous (aq.) HCl. FDNP-alanamide was used as a solution in acetone (33 mM). In a 2-mL vial, the amino acid (2.5 μL, 0.50 μmol) was diluted in 1 M aq. $NaHCO_3$ (67 μL). FDNP-alanamide (30 μL, 1 μmol) was added, and then the vial was immersed in an oil bath that had been equilibrated to 40 °C. After 12 h, the reaction mixture was allowed to cool to room temperature, and then diluted with 1:1 water/acetonitrile (900 μL). The resulting solution was subjected to centrifugation (20,000 × *g*, 4 °C, 5 min). The supernatant was analyzed directly by LC-MS. Each amino

acid was derivatized with both racemic and enantiopure FDNP-alanamide for comparison. All amino acid products were enantiopure. Absolute stereochemistry was inferred by analogy to L-tryptophan.

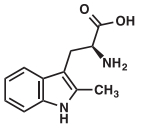

^{1}H NMR (400 MHz, CD_3OD) δ 7.60 (d, J = 7.1 Hz, 1H), 7.26 (d, J = 7.4 Hz, 1H), 7.06–6.97 (m, 2H), 3.83 (dd, J = 9.9, 4.2 Hz, 1H), 3.26 (**AB**X, J_{AX} = 9.9 Hz, J_{BX} = 4.2 Hz, J_{AB} = 15.2 Hz, ν_{AB} = 164.0 Hz, 2H), 2.42 (s, 3H). **LRMS** (ESI) (*m/z*) for $[M+H]^+$ $C_{12}H_{15}N_2O_2$ requires 219.1, observed 219.1.

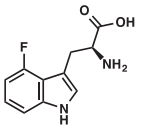

^{1}H NMR (300 MHz, DMSO-d_6) δ 11.40 (s, 1H), 7.23 (s, 1H), 7.18 (d, J = 8.1 Hz, 1H), 7.00 (td, J = 7.9, 5.2 Hz, 1H), 6.69 (ddd, J = 11.5, 7.8, 0.8 Hz, 1H), 3.52–3.36 (m, 2H), 2.90 (dd, J = 15.8, 11.1, 1H). **^{19}F NMR** (282 MHz, DMSO-d_6) δ –124.26 (dd, J_{F-H} = 11.3, 5.2 Hz). **LRMS** (ESI) (*m/z*) for $[M+H]^+$ $C_{11}H_{12}FN_2O_2$ requires 223.1, observed 223.1.

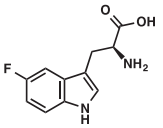

^{1}H NMR (300 MHz, DMSO-d_6) δ 11.19 (s, 1H), 7.36–7.25 (m, 3H), 6.87 (td, J = 9.2, 2.5 Hz, 1H), 3.37 (dd, J = 7.5, 4.1, 1H), 3.04 (**AB**X, J_{AX} = 8.1 Hz, J_{BX} = 4.2 Hz, J_{AB} = 14.6 Hz, ν_{AB} = 85.8 Hz, 2H). **^{19}F NMR** (282 MHz, DMSO-d_6) δ –125.84 (td, J_{F-H} = 9.8, 4.6 Hz). **LRMS** (ESI) (*m/z*) for $[M+H]^+$ $C_{11}H_{12}FN_2O_2$ requires 223.1, observed 223.1.

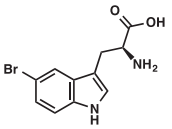

^{1}H NMR (400 MHz, CD_3OD) δ 7.91 (d, J = 1.8 Hz, 1H), 7.29 (d, J = 8.5 Hz, 1H), 7.23 (s, 1H), 7.21 (dd, J = 8.6, 1.9 Hz, 1H), 3.82 (dd, J = 9.1, 4.1 Hz, 1H), 3.29 (**AB**X, J_{AX} = 9.1 Hz, J_{BX} = 4.2 Hz, J_{AB} = 15.2 Hz, ν_{AB} = 124.0 Hz, 2H). **LRMS** (ESI) (*m/z*) for $[M+H]^+$ $C_{11}H_{12}BrN_2O_2$ requires 283.0 and 285.0, observed 283.0 and 285.0.

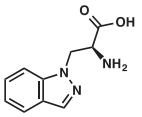

As the HCl salt: **^{1}H NMR** (400 MHz, D_2O) δ 8.16 (s, 1H), 7.84 (d, J = 8.2 Hz, 1H), 7.62 (d, J = 8.6 Hz, 1H), 7.52 (t, J = 7.7 Hz, 1H), 7.25 (t, J = 7.5 Hz, 1H), 4.99 (**AB**X, J_{AX} = 4.1 Hz, J_{BX} = 6.0 Hz, J_{AB} = 15.6 Hz, ν_{AB} = 44.0 Hz, 2H), 4.54 (dd, J = 6.0, 4.1 Hz, 1H). **LRMS** (ESI) (*m/z*) for $[M+H]^+$ $C_{10}H_{12}N_3O_2$ requires 206.1, observed 206.1.

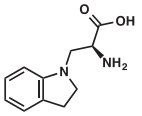

As the HCl salt: **^{1}H NMR** (400 MHz, D_2O) δ 7.22 (d, J = 7.3 Hz, 1H), 7.16 (t, J = 7.7 Hz, 1H), 6.83 (t, J = 7.4 Hz, 1H), 6.70 (d, J = 7.9 Hz, 1H), 4.25 (q, J = 6.0 Hz, 1H), 3.70–3.56 (m, 2H), 3.46 (q, J = 8.3 Hz, 1H), 3.37 (q, J = 8.4 Hz, 1H), 3.00 (t, J = 8.2 Hz, 2H). **LRMS** (ESI) (*m/z*) for $[M+H]^+$ $C_{11}H_{14}N_2O_2$ requires 207.1, observed 207.1.

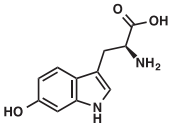

^{1}H NMR (400 MHz, DMSO-d_6) δ 10.48 (d, J = 2.2 Hz, 1H), 7.30 (d, J = 8.5 Hz, 1H), 6.95 (d, J = 2.2 Hz, 1H), 6.69 (d, J = 2.1 Hz, 1H), 6.51 (dd, J = 8.5, 2.1 Hz, 1H), 3.38 (dd, J = 9.2, 3.6 1H), 3.02 (**AB**X, J_{AX} = 9.1 Hz, J_{BX} = 3.8 Hz, J_{AB} = 15.0 Hz, ν_{AB} = 155.5 Hz, 2H). **LRMS** (ESI) (*m/z*) for $[M+H]^+$ $C_{11}H_{13}N_2O_3$ requires 221.1, observed 221.1.

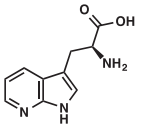

^{1}H NMR (300 MHz, D_2O) δ 8.16 (dd, J = 5.0, 1.4 Hz, 1H), 8.06 (dd, J = 7.9, 1.5 Hz, 1H), 7.31 (s, 1H), 7.13 (dd, J = 7.9, 4.9 Hz, 1H), 3.96 (dd, J = 7.3, 5.1 Hz, 1H), 3.30 (**AB**X, J_{AX} = 7.3 Hz, J_{BX} = 5.2 Hz, J_{AB} = 15.4 Hz, ν_{AB} = 33.0 Hz, 2H). **LRMS** (ESI) (*m/z*) for $[M+H]^+$ $C_{10}H_{12}N_3O_2$ requires 206.1, observed 206.1.

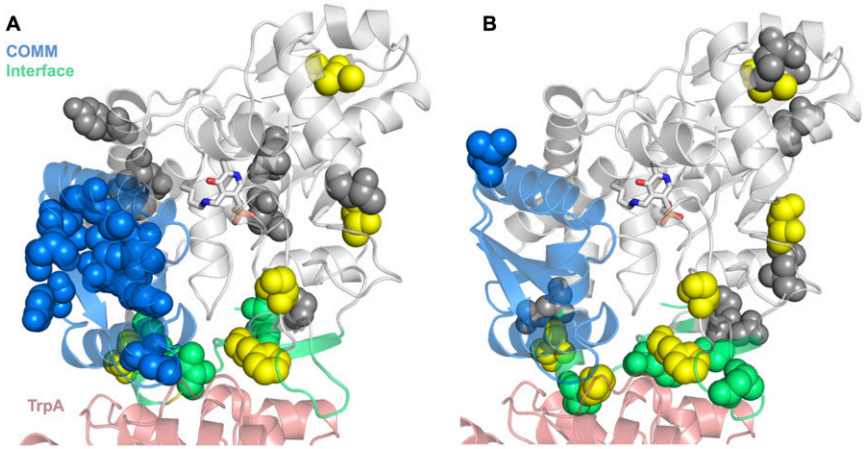

Fig. S1. Distribution of activating mutations identified through random mutagenesis and screening. (*A*) Positions on *Pf*TrpB where activating mutations were discovered are displayed as spheres. The mutations are W2R, G4C, V11A, E17G, K20E, E23V, F35S, N35S, Y41C, I68V, M123V, I127S, M144T, N150T, N166D, Y178C, H180R, Y181C, L182P, M233V, M233I, F274S, F274L, D284G, T292S, T321A, and T323A. Mutations located in the COMM domain are colored blue, those within 5 Å of *Pf*TrpA (red) are cyan, those present in *Pf*TrpB^{4D11} are yellow, and the remainder are gray. (*B*) Positions on *Pf*TrpB where activating mutations were discovered using *Pf*Trp^{4D11} as the parent for random mutagenesis. The mutations are G4D, E5K, Y10H, P12L, E13G, E21V, L59Q, K67I, L146V, D220E, N267S, G272D, and D284E. Color scheme is the same as *A*; yellow spheres are mutations present in the final variant *Pf*TrpB^{0B2}.

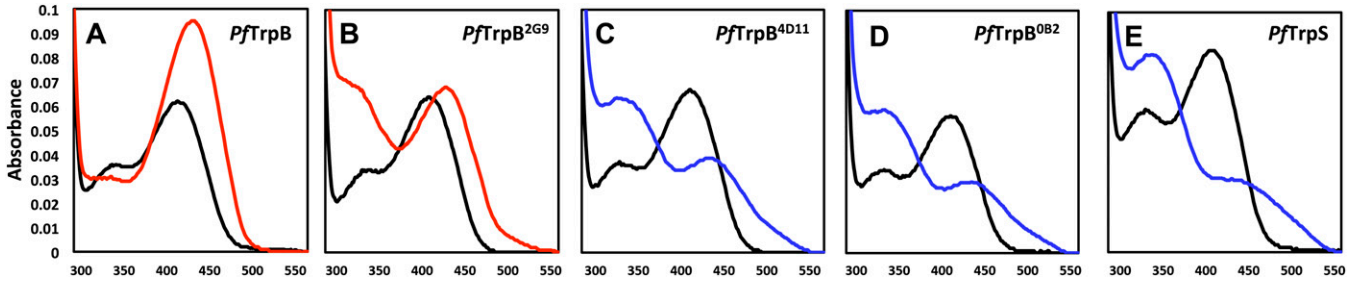

Fig. S2. UV-vis absorption spectra for native and engineered TrpB. *A*, *D*, and *E* are the same as in Fig. 2. PLP absorption spectra for each enzyme are shown in black and share $\lambda_{max} = 412$ nm, characteristic of E(Ain). Addition of 20 mM L-Ser causes a red-shift to 420 nm (red), consistent with E(Aex_1) formation for *Pf*TrpB and *Pf*TrpB^{2G9} (*B*), which also has an absorbance band at ~320 nm that we attribute to formation of pyruvate through serine deaminase activity. L-Ser addition to *Pf*TrpS, *Pf*TrpB^{4D11} (*C*), and *Pf*TrpB^{0B2} causes a shift in λ_{max} to 350 nm and a broad shoulder extending to 550 nm. The 350-nm absorption is attributed to the E(A-A), and the shoulder indicates a mixed population of E(Aex_1) and E(A-A). All spectra collected with 20 μM enzyme. To limit the amount of pyruvate production, spectra were taken as quickly as possible (<10 s) after addition of L-Ser.

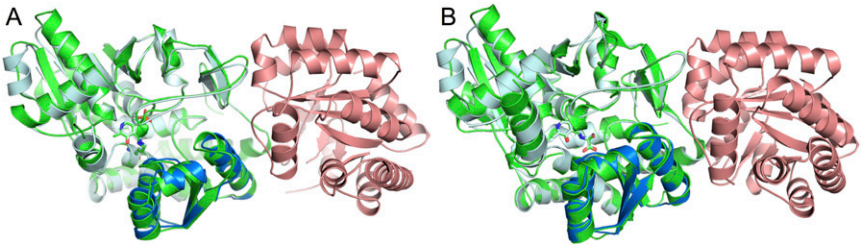

Fig. S3. Structural comparison between *St*TrpS and *Pf*TrpB in E(Ain) and E(Aex_1) forms. (*A*) Alignment of *St*TrpB (green; PDB ID code 1BKS) and *Pf*TrpB (light blue) in their substrate-free [E(Ain)] forms yields an rmsd of 0.5 Å. Small differences exist in the structures near the α-subunit (red) binding site, and the COMM domain of *Pf*TrpB (dark blue) is in a slightly more open conformation than for *St*TrpB. (*B*) Alignment of *St*TrpB (green; PDB ID code 2CLL) and *Pf*TrpB (light blue) with L-serine covalently bound as the external aldimine, E(Aex_1), yields an rmsd of 0.5 Å.

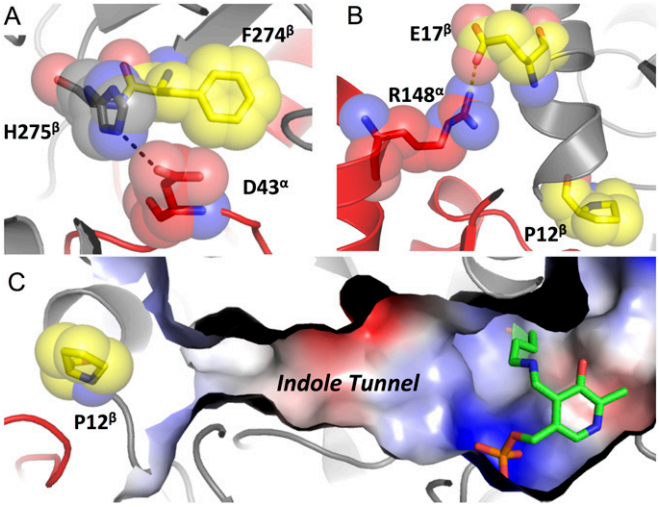

Fig. S4. Interactions between *Pf*TrpA and *Pf*TrpB that are disrupted in *Pf*TrpB^{0B2}. (*A*) Hydrogen bond between H275$^{\beta}$ (gray) and D43$^{\alpha}$ (red) in the gate-open conformation is adjacent F274$^{\beta}$ (yellow), which is mutated to Ser in the *Pf*TrpB^{4D11} and *Pf*TrpB^{0B2} enzymes. (*B*) A salt bridge (dashes) between R148$^{\alpha}$ (red) and E17$^{\beta}$ (yellow) is removed with the E17G mutation present in *Pf*TrpB^{4D11} and *Pf*TrpB^{0B2}. P12$^{\beta}$ is located along the indole tunnel (*C*) between the subunits. Steric constraints indicate that the P12L mutation of *Pf*TrpB^{0B2} would disrupt this tunnel, which might contribute to the large drop in Trp synthase activity of *Pf*TrpS^{0B2}.

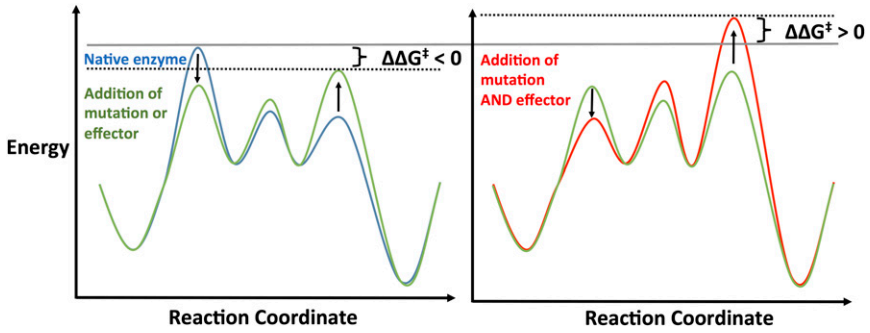

Fig. S5. Hypothetical reaction coordinate diagram to illustrate inversion of TrpA effector activation to inhibition. Native enzyme, such as TrpB (blue), with multiple reaction transition states. Effector addition or introduction of mutations (green) increases the rate of the reaction by lowering the free energy of the rate-limiting step (RLS), while simultaneously raising the energy of a different transition state thereby generating a new RLS. The same changes applied a second time (red), as might occur with *Pf*TrpA addition to the engineered TrpB, can lead to a free-energy barrier higher than for the native enzyme and a reduction in overall reaction rate.

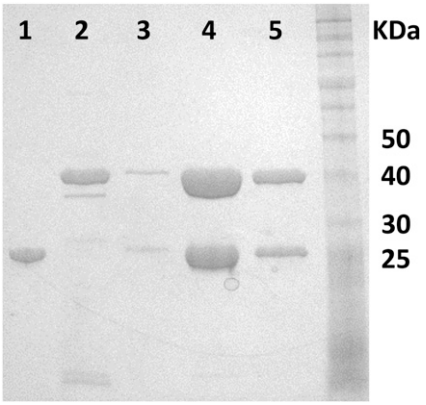

Fig. S6. SDS/PAGE of *Pf*TrpA, *Pf*TrpB, and *Pf*TrpS. 1, *Pf*TrpA; 2, *Pf*TrpB; 3–5, aliquots from 1.5-mL fractions from *Pf*TrpA pull-down using His-tagged *Pf*TrpB; 4–20% gradient, SDS/PAGE. Molecular weights from ColorPlus Prestained Protein Ladder (New England Biosystems) listed on the right.

Table S1. Comparison of TrpB thermophilic enzymes

Host	k_{cat}, s^{-1}	K_M, mM L-Ser	K_M, μM indole	k_{cat} change with TrpA	Thermal stability indicators	Ref(s).
Thermotoga maritima	4.2	110	40	2.4	Kinetics measured at 80 °C	18
Thermococcus kodakarensis	1.04 ± 0.03	n/a	63 ± 5	3.3	5% activity after 1 h at 80 °C	19
Pyrococcus furiosus	0.31 ± 0.02	1.2 ± 0.1	77 ± 12	3.2	T_{50} = 94.7 ± 1.2	20–22

Values for *Pf*TrpB are those reported here; the references supply similar data measured by a different group. n/a, not available.

Table S2. Biochemical characterization of native and engineered enzymes

Enzyme	Mutations	k_{cat}, s^{-1}	K_M, mM L-Ser	K_M, μM indole	k_{cat}/K_M, $mM^{-1}{\cdot}s^{-1}$ (Ind)	k_{cat} change with TrpA	T_{50} °C
*Pf*TrpS	–	1.0 ± 0.1	0.6 ± 0.1	20 ± 2	50	–	>95
*Pf*TrpB	–	0.31 ± 0.02	1.2 ± 0.1	77 ± 12	4	3.2	95.1 ± 1.3
*Pf*TrpB^{2G9}	T292S	1.1 ± 0.2	0.84 ± 0.04	14 ± 3	78	0.34	94.7 ± 1.2
*Pf*TrpB^{4D11}	E17G, I28V, F274S, T292S, T321A	2.2 ± 0.2	1.2 ± 0.2	11 ± 2	200	0.3	83.6 ± 2.4
*Pf*TrpB^{0B2}	P12L, E17G, I28V, F274S, T292S, T321A	2.9 ± 0.2	0.7 ± 0.1	8.7 ± 1.8	330	0.04	87.3 ± 1.3

Assay parameters are described in *SI Materials and Methods*.

Table S3. Crystallographic data collection and refinement statistics

Protein	*Pf*TrpB	*Pf*TrpB	*Pf*TrpB	*Pf*TrpS
PDB ID code	5DVZ	5DW0	5DW3	5E0K
Ligand	None	L-Serine	L-Tryptophan	None
Space group	$P2_12_12_1$	$P2_12_12_1$	$P2_12_12_1$	$P2_12_12_1$
Cell dimensions, Å	a,b,c = 87.1, 111.9, 160.8	a,b,c = 84.2, 109.1, 160.8	a,b,c = 83.7, 108.9, 160.1	a,b,c = 87.7, 225.0, 296.2
Cell angles	$\alpha = \beta = \gamma = 90°$	$\alpha = \beta = \gamma = 90°$	$\alpha = \beta = \gamma = 90°$	$\alpha = \beta = \gamma = 90°$
Data collection				
Wavelength, Å	0.9795	0.9795	0.9795	0.9795
Beamline	SSRL 12.2	SSRL 12.2	SSRL 12.2	SSRL 12.2
Resolution, Å	40–1.69	40–2.01	40–1.74	40–2.76
Last bin (Å)	(1.72–1.69)	(2.05–2.01)	(1.77–1.74)	(2.81–2.76)
No. observations	865,034	942,945	1,455,851	1,006,477
Completeness (%)	99.6 (99.9)	98.0 (67.2)	98.7 (75.0)	99.3 (93.7)
R_{pim} (%)	0.050 (0.899)	0.034 (0.754)	0.020 (0.752)	0.082 (1.21)
CC(1/2)	0.995 (0.439)	0.999 (0.299)	1.000 (0.425)	0.990 (0.154)
I/σI	7.3 (0.6)	15.1 (0.9)	18.0 (1.0)	8.0 (0.6)
Redundancy	4.9 (4.9)	9.8 (5.6)	9.8 (2.8)	6.7 (5.3)
Refinement				
Total no. of reflections	161,910	91,540	140,124	142,144
Total no. of atoms	12,278	11,976	12,282	28,872
Final bin (Å)	(1.73–1.69)	(2.07–2.01)	(1.79–1.74)	(2.83–2.76)
R_{work} (%)	20.2 (39.1)	17.6 (36.7)	18.9 (36.1)	20.4 (37.7)
R_{free} (%)	22.8 (39.0)	22.1 (36.8)	22.7 (38.4)	23.8 (39.2)
Average B factor, $Å^2$	31.8	42.7	40.5	
Ramachandran plot favored, %	96.8	96.2	96.6	97.3
Allowed, %	100	100	99.9	99.8
Outliers, %	0	0	0.1	0.2

Values in parentheses are for the highest-resolution shell. R_{merge} is $\Sigma|Io - I|/\Sigma Io$, where Io is the intensity of an individual reflection, and I is the mean intensity for multiply recorded reflections; R_{work} is $\Sigma||Fo - Fc||/Fo$, where Fo is an observed amplitude and Fc a calculated amplitude; R_{free} is the same statistic calculated over a 5% subset of the data that has not been included.